Published in final edited form as:
J Comp Neurol. 2014 July 1; 522(10): 2299–2318. doi:10.1002/cne.23535.

Calretinin and calbindin distribution patterns specify subpopulations of type I and type II spiral ganglion neurons in postnatal murine cochlea

Wenke Liu and **Robin L. Davis**
Department of Cell Biology and Neuroscience, Rutgers University, Piscataway, NJ, 08854, USA

Abstract

As the first neural element in the auditory pathway, neurons in the spiral ganglion shape the initial coding of sound stimuli for subsequent processing. Within the ganglion, type I and type II neurons form divergent and convergent innervation patterns, respectively, with their hair cell sensory receptors, indicating that very different information is gathered and conveyed. Layered onto these basic innervation patterns are structural and electrophysiological features that provide additional levels of processing multifaceted sound stimuli. To understand the nature of this additional complexity of signal coding, we characterized the distribution of calretinin and calbindin, two regulators of intracellular calcium that serve as markers for neuronal subpopulations. We showed in acute preparations and *in vitro* that calretinin and calbindin staining levels were heterogeneous. Immunocytochemical analysis of co-localization further showed that high levels of staining for the two molecules rarely overlapped. Although varied amounts of calbindin and calretinin were found within each tonotopic location and neuronal type, some distinct sub-distributions were noted. For example, calretinin levels were highest in neurons innervating the mid-cochlea region, whereas calbindin levels were similar across the entire ganglion. Furthermore, we noted that apical type II neurons, identified by anti-peripherin labeling had significantly lower levels of calretinin and higher levels of calbindin. We also established that the endogenous firing feature of onset tau of the sub-threshold response showed a pattern related to quantified calretinin and calbindin staining levels. Taken together, our results are suggestive of an additional dimension of complexity within the spiral ganglion beyond that currently categorized.

Keywords

calretinin; calbindin; spiral ganglion

Corresponding author: Dr. Robin L. Davis, Department of Cell Biology & Neuroscience, 604 Allison Road, Nelson Laboratories, Rutgers University, Piscataway, NJ 08854, rldavis@rci.rutgers.edu Phone: 732-445-0440, FAX: 732-445-5870.
Role of authors: All authors had full access to all the data in the study and take responsibility for the integrity of the data and the accuracy of the data analysis. RLD designed the concept of the study and supervised the project. WL acquired and analyzed the data. RLD and WL interpreted the data and wrote the manuscript.

Conflict of interest statement: The authors declare no conflict of interest.

Introduction

To achieve accurate and rapid representation of the external environment, a common theme in sensory systems is to separate and sort sub-modalities of sensory input into distinct neuronal pathways, which are initially defined by the structural and physiological characteristics of the peripheral receptors and primary afferents. Evidence for this type of organization, which underlies parallel processing has been well described in the visual, olfactory and somatosensory systems (Field and Chichilnisky, 2007; Leinwand and Chalasani, 2011; Ma, 2012). In the retina, for example, there are distinct cell types and separate neural circuits organized to restructure visual information into light intensity, color contrast and motion (Gollisch and Meister, 2010). In the olfactory system, in addition to the classic chemotopic organization in which mitral/tufted cells in different glomeruli of olfactory bulb receive projections from olfactory sensory neurons expressing different types of odorant receptors, an additional dimension of parallel processing is represented by mitral/tufted cells in each glomerulus that encode non-redundant odor information (Dhawale et al., 2010). In the somatosensory system, parallel processing is represented by different receptors and afferent fibers that code distinct sub-modalities of body senses such as touch, pain, itch, and temperature (Reed-Geaghan and Maricich, 2011).

The perception of sound involves modalities such as pitch, loudness, timbre and location (Bizley and Walker, 2010), all of which are spectral- and temporal-related, and may require complex central processing as well as detailed peripheral encoding. In contrast to other sensory pathways, there is very little known about how parallel pathways are represented in the primary afferents of the auditory system. In the cochlea, the relatively well characterized coding mechanism is the frequency discrimination that arises from cochlear specializations that form a tonotopic map, in which mechanical and physiological properties of the basilar membrane, the hair cells receptors and the ribbon synapses are tuned along the cochlea, such that distinct regions optimally respond to a defined sound frequency (Slepecky, 1996; Meyer et al., 2009). There are also indications of an intensity coding mechanism that may contribute to the perception of different levels of loudness. Early studies of cat auditory nerve fibers using *in vivo* recording and retrograde labeling revealed that the neural responses of auditory afferents in the same frequency region are highly varied in terms of intensity-related parameters such as spontaneous discharge rate, threshold, and dynamic range (Liberman, 1978).

Primary auditory afferents are classified into categories of type I and type II neurons, which innervate inner and outer hair cells, respectively (Ryugo, 1992). Interestingly, in contrast to the visual, olfactory and somatosensory systems in which distinct receptor types and local circuitry are explicitly committed to different modalities, the functional significance of two distinct type I and type II pathways remains largely unknown. Most *in vivo* recordings have been made from the type I fibers that compose 95% percent of the neuronal population, while very little data has been obtained from the small, unmyelinated type II fibers. It is clear that it is the type I neurons that are primarily responsible for auditory sensation (Liberman, 1982; Keithley and Schreiber, 1987; Ruggero, 1992), whereas the exact contribution of the type II neurons to audition is under dispute (Brown, 1994; Robertson, 1984; Reid et al., 2004; Weisz et al., 2009). Beyond the type I and II dichotomy, very little

is known about potential subpopulations in each category. This is in contrast to the striking heterogeneity of cell types with distinct morphological and physiological features in other sensory organs (Wässle, 2004; Marmigère and Ernfors, 2007; Angelo et al., 2012). Thus, much remains to be learned about this primary afferent element and the fundamental characteristics of possible neuronal subtypes that could underlie processing of auditory stimuli.

Toward this goal we utilized the calcium binding proteins calretinin and calbindin, which have been used to characterize cell specifications in the brain as well as in sensory systems. In the retina, heterogeneous levels of calretinin and calbindin immunocytochemical labeling reflect the highly organized and complex structure in the inner plexiform layer (Haverkamp and Wässle, 2000; Wässle, 2004). Moreover, there is evidence that calretinin and calbindin are differentially distributed in rat amacrine cells and retinal ganglion cells (Mojumder et al., 2008) suggesting that these calcium binding proteins subserve different functions. Therefore, examination of the distribution of calretinin and calbindin may help to elucidate the structural and physiological basis for possible parallel pathways in the spiral ganglion.

In the present study we sought to determine the relationship between the amount and type of calcium binding protein present in spiral ganglion neurons and the accompanying functional impact. Our results show that both calretinin and calbindin are distributed heterogeneously in the postnatal spiral ganglion *in vitro*, the relative amounts of which correlate with one intrinsic firing parameter, the onset tau of sub-threshold responses. Calretinin is highest in the type I neurons in the mid-cochlear region and type II spiral ganglion neurons in the apex were shown to possess the highest levels of calbindin and lowest levels of calretinin. Thus, anti-calretinin and anti-calbindin immunolabeling revealed an additional layer of heterogeneity in both type I and type II spiral ganglion neurons, indicating another dimension of specification that may contribute to the complex signaling capacity of the spiral ganglion.

Materials and Methods

Tissue Culture

Procedures performed were approved by the Rutgers University Institutional Review Board for the Use and Care of Animals. Cochleae were removed from postnatal day 6 to 7 (P6-7) CBA/CaJ mice that were euthanized by decapitation and either plated on poly-L-lysine coated culture dishes or prepared as paraffin embedded sections. For *in vitro* neuronal cultures, uncoiled spiral ganglia from P6-7 mice were divided into five parts and three of them, from the apical, middle and basal regions were isolated into separate culture dishes. All preparations were maintained in growth medium: DMEM (Sigma) supplemented with 10% fetal bovine serum, 4 mM L-glutamine, and 0.1% penicillin–streptomycin. All culture dishes were maintained at 37°C in a humidified incubator with 5% CO_2 and were used at DIV6-7. The period of time *in vitro* was extended to 6-7 days, such that the neurons in the culture were rendered to electrophysiological recordings, and data obtained in these cultures reflect early postnatal animals in a broad scope. Cochlear whole-mounts were dissected from P6-P7 mice and subjected to fixation and staining immediately.

Paraffin-embedded Sections

The temporal bones were dissected from P6-P7 CBA/CaJ mice and fixed with 4% paraformaldehyde for 2 hours at room temperature with gentle shaking, and were kept in 1X PBS at 4°C overnight. On the next day, the tissue was embedded in paraffin and sectioned at 4-6μm. All sections were collected on poly-L-lysine coated glass slides and let dry overnight. Before immunohistochemical staining, the paraffin-embedded sections were deparaffinized in Histoclear (National Diagnostics) for 20 minutes and were rehydrated in 100%, 95%, 85%, 75%, 50% ethanol and distilled H_2O each for 5 minutes. Finally, the sections were treated with Target Retrieval Solution (DAKO) at 95°C for 20 minutes, rinsed with 0.01M PBS 3X prior to immunohistochemical staining.

Antibody Characterization

Antibodies utilized in the study for immunocytochemical analyses are summarized in Table 1.

Anti-class III β-tubulin antibody—Monoclonal mouse anti-class III β-tubulin antibody (Tuj1, Covance, MMS-435P) was used at 1:200 dilution to obtain a general labeling of all spiral ganglion neurons in paraffin-embedded sections, cochlear whole-mounts and neuronal cultures. The antibody was used in previous studies from the lab (Reid et al., 2004; Flores-Otero and Davis, 2011) and showed a specific labeling of cytoskeleton in spiral ganglion neurons.

Anti-calretinin antibodies—Pre-adsorption and Western blots evaluations of polyclonal rabbit anti-calretinin (Millipore, AB5054) and monoclonal mouse anti-calretinin (Millipore, MAB1568) antibodies have been used to determine their specificity for calretinin (Baizer and Broussard, 2010; Fuentes-Santamaria et al., 2005). We further validated the specificity of both antibodies in mouse using Western blot following standard protocols. In brief, P7 mouse brain lysates were run through 10% SDS-PAGE and then transferred to a PVDF membrane (Bio-Rad). The membrane was then incubated with primary antibody at 4°C overnight. Horseradish peroxidase conjugated secondary antibodies against either mouse or rabbit IgG (Amersham) were used at 1:5000. The immunoblot bands were visualized with chemiluminescence (ECL-SuperSignal West Pico Chemilunimescence Substrate, Pierce). The total protein loaded in each blot was visualized by staining using 2% Comassie blue solution. The rabbit polyclonal and the mouse monoclonal antibodies were used with 1:6000 and 1:2000 dilutions and each showed a single band of the expected molecular weight of 29kDa (Schwaller, 2009), indicating that they specifically recognized the appropriate protein.

Anti-calbindin antibody—Polyclonal rabbit anti-calbindin (Swant, CB38) antibody, applied to calbindin knockout tissue, showed no signal in both a Western blot and immunostaining (Airaksinen et al., 1997). We further validated the specificity with a Western blot at a 1:6000 dilution. The antibody recognized a band at the expected molecular weight of 28kDa (Schwaller, 2009). Co-labeling experiments using both the monoclonal anti-calretinin antibody and the polyclonal anti-calbindin antibody reveal distinct patterns (see results section), indicating that each antibody recognized distinct proteins.

Anti-peripherin antibody—Monoclonal mouse anti-peripherin antibody (Chemicon, MAB1527) was used as a marker for type II spiral ganglion neurons according to previous reports (Mou et al., 1998; Reid et al., 2004). The appropriate concentration of anti-peripherin antibody was determined using a preparation in which the organ of Corti and the ganglion were cultured for 3 days *in vitro*, such that the type I and type II afferent innervations patterns were retained and could be distinguished using anti-peripherin antibody staining (Flores-Otero and Davis, 2011). Because anti-peripherin antibody also labels type I neurons in the apex when concentrations are too high or fails to label all type II neurons in the base when the concentrations are too low, we utilized the organ of Corti cultures to establish working concentrations that were optimized for different tonotopic regions (1:6000 for apex, 1:5000 for middle and 1:4000 for base).

Immunohistochemistry

For cochlear whole-mounts and neuronal cultures, preparations were fixed and permeabilized with 100% methanol at −20°C for 6 min and rinsed three times with 0.01M PBS (pH 7.4). Before the application of antibodies, specimens were incubated with 5% normal goat serum (NGS) for 1h at RT or 4°C overnight. Specimens were incubated with primary antibodies at either 4°C overnight (peripherin, calretinin and calbindin) or at RT for 1h (β-tubulin). Monoclonal mouse anti-β-tubulin (1:200, Covance, MMS 435P) was used to label all neurons and monoclonal mouse anti-peripherin (Chemicon, MAB1527) antibody to specifically identify putative type II spiral ganglion neurons. Polyclonal rabbit anti-calretinin (Millipore, AB5054) was used at 1:200. Polyclonal rabbit anti-calbindin (Swant, CB38) and monoclonal mouse anti-calretinin (Millipore) antibodies were used at 1:100. After washing 3X with PBS the preparations were incubated with 5% NGS for 1h at RT and then with one of the following secondary antibodies at 1:100 for 1h at RT: Alexa Fluor 594 conjugated goat anti-mouse; Alexa Fluor 488 conjugated goat anti-rabbit, Alexa Fluor 350 conjugated goat anti-mouse (Invitrogen). Multi-antibody-labeling was done sequentially. At the end of all the staining steps the preparations were washed with 0.01M PBS and mounted in DABCO medium (Sigma-Aldrich).

Image Acquisition

Images of neuronal cultures were acquired with a fluorescent microscope (Zeiss) and camera (Hamamatsu 1394 ORCA-ER) using IPLab Scientific Imaging software (BD Biosciences). Immunolabeled cochlear whole-mounts were visualized using a LSM 510 confocal microscope (Zeiss) with 10X and 63X water immersion DIC objectives. Some images were adjusted by brightness and contrast using IPLab, LSM Image Browser (Zeiss) and Adobe Photoshop software for presentation purposes as previously described (Flores-Otero et al., 2007).

Staining Irradiance Analysis

At least 3 experiments were used for each quantitative evaluation. A single experiment was composed of multiple measurements from individual neurons (usually more than 200 per experiment) from apical, middle and basal explants isolated from two cochleae. Immunostaining irradiance against the protein of interest was quantified and combined using

the following analysis: Exposure time of each color channel was fixed within a single experiment to enable internal comparison. Staining against the neuronal marker β-tubulin, which exhibited a relatively uniform pattern throughout the ganglion, was used in all experiments to obtain a general reference image, which confirmed that the differential levels of calretinin and calbindin staining could not be attributed to differences in antibody penetration (Fig. 1). For cytoskeleton anti-peripherin staining, the fluorescence intensity was sampled by a box tool with an area of 36 pixels in the region of interest on an acquired image using IPLab software. The staining irradiance value of a neuron was determined by subtracting the average of four surrounding background measurements from the average of three measurements in the brightest area in the soma. For antibodies that stain both the cytoplasm and the nucleus, the staining irradiance value of each cell was determined by the average irradiance over the entire soma and then subtracting the average of four surrounding background measurements with the box tool. Only rarely did the cytoplasmic irradiance differ from the nuclear levels (Fig. 1, arrow), ensuring that averaging over the entire cell soma yielded an accurate overall evaluation of staining levels. The normalized staining irradiance of a neuron was represented by the ratio of its measured fluorescent intensity to that obtained from the brightest neuron in the same experiment. In some of the experiments, electrophysiological recordings were made prior to immunostaining. Hoffman modulation contrast images of each recorded neuron were taken to document cell position and care was taken to re-identify the recorded neurons in the staining images with the aid of unique marking on the dish (Reid et al., 2004). All dishes within a single experiment from which recordings were obtained were visualized for immunostaining with the same exposure time. In order to compare levels across individual experiments, the staining irradiance of each neuron was normalized to the brightest cell in the group of samples that underwent the same staining procedure.

Electrophysiology

Recordings were made with glass pipettes (Sutter Instruments, cat.# BF 150-110-10) pulled on a vertical puller (Narishige, model# PP-83) and coated with Sylgard (Dow Corning). Pipette tips were fire-polished immediately before use and resistances ranged from 3 to 10MΩ. All data were collected at room temperature from neuron somata, and pipette offset currents were zeroed just before contacting the cell surface. Recordings were made with Axopatch 200A amplifier (Axon Instruments) and I_{fast} circuitry was used for whole-cell current clamp mode. Data were digitized at 5kHz and filtered at 1kHz. Programs of data acquisition and analysis were generously contributed by Dr. Mark Plummer, Rutgers University. Pipettes were filled with the following internal solution: 112mM KCl, 0.1mM $CaCl_2$, 2mM $MgCl_2$, 11mM EGTA, 10mM HEPES, pH 7.5. Neurons were exposed to the following bath solution: 136.9mM NaCl, 5.4mM KCl, 1.67mM $CaCl_2$, 0.98mM $MgCl_2$, 16.7mM glucose, 50mM sucrose, 10mM HEPES, pH 7.5. Current clamp recordings were considered of acceptable quality if they met the following criteria: the amplitude of the first action potential exceeds 70mV, stable membrane potentials, low noise levels and discernible membrane time constant on step current injection. If any of the parameters changed during a recording, the remainder of the data was excluded due to an indication of compromised cell integrity. After recording, the pipette was carefully withdrawn and the neuron culture was fixed and evaluated with immunohistochemistry.

Measurement of Intrinsic Firing Parameters

Prior to entering the whole-cell current clamp configuration, the endogenous resting membrane potential of each neuron was assessed non-invasively (Verheugen et al., 1999). In brief, single K^+ channel activity was recorded to voltage steps from −100mV to −20mV from a holding potential of −60mV, with standard internal solution in the pipette (Fig. 2A-B). Due to the relatively high concentration of K^+ across the cell membrane, the resting membrane potential was determined as the reversal potential from the I-V relationship of a K^+ channel (Fig. 2C). K^+ selective channels with conductances in the range of 35-50pS, which were observed most frequently in our recordings, were used to calculate the resting membrane potential. In some recordings, channel openings with large amplitudes (Fig. 2B, arrowhead) were also observed and reversed at a similar potential as the 35-50pS channels (Fig. 2b, arrow), consistent with the reported presence of the BK channel in the murine spiral ganglion (Adamson et al., 2002). Subsequent to single channel recording and on-line resting membrane potential calculation, the cell was held at its endogenous resting membrane potential in current clamp mode. Threshold level was reached when the same depolarization conditions fluctuated between just sub-threshold activity and an action potential. Voltage threshold was determined as the peak voltage level (Fig. 2D, arrow) of the just sub-threshold trace (Fig. 2D, black); differential voltage was defined as the voltage difference between holding potential and voltage threshold. Onset tau was determined from a double-exponential fit to the sub-threshold trace. Width of a supra-threshold action potential (Fig. 2D, gray) measured at the mid height between the peak and nadir was measured as duration (half-width) and the time difference between stimulus onset and the peak of the action potential was determined as firing latency. The neuron was then depolarized to supra-threshold voltage levels until the maximum number of spikes occurred and AP max was documented (Mo and Davis, 1997) .

Statistical analysis

Average data were presented as mean ± standard error of means (SEM). One-way ANOVA was carried out to determine differences among groups of data followed by *post hoc* analysis. Student's *t*-test (for comparing two groups) or Tukey's honestly significant difference (HSD) test (for the comparison of multiple groups) were used to calculate *p* values. The Kolmogorov-Smirnov test was used to compare the distribution of two samples and the *p* value calculation was based on a two-sided assumption.

Results

Heterogeneous distribution of calretinin and calbindin in the spiral ganglion

Calretinin and calbindin, widely used as markers for neuronal subpopulations in the central nervous system and in the vestibular ganglion, (DeFelipe, 1997; Kevetter, 2002; Leonard and Kevetter, 2002) are also present in the embryonic and postnatal mouse spiral ganglion (Dechesne and Thomasset, 1988; Dechesne et al., 1994). In order to determine whether sub-classes of auditory afferents could be identified by calcium binding protein distributions we characterized the distribution patterns of calretinin and calbindin within and throughout the ganglion in postnatal day 6-7 (P6-7) CBA/CaJ mice, at a well-characterized stage of

development (Mo and Davis, 1997; Adamson et al., 2002; Reid et al., 2004) when afferent innervation in the cochlea has been established (Huang et al., 2007).

As a first step, acute preparations were utilized to determine the intra-ganglion spatial organization and intracellular co-localization of anti-calretinin and anti-calbindin antibodies. Observations of anti-calretinin antibody in postnatal cochlear sections in which the structural detail of the cochlea was retained showed that the hair cells (Fig. 3A) and neuronal cell bodies in the spiral ganglion and afferent fibers (Fig. 3B-E) were strongly labeled. By comparison, anti-calbindin antibody labeling had distinctly lower irradiance levels in the cell bodies of spiral ganglion neurons compared to the hair cells within the same section (Fig. 3F-J). Despite their relatively different staining levels when compared to the hair cells, we found that both calretinin and calbindin labeling was heterogeneous in spiral ganglion neurons. Neighboring neurons in the same region of the ganglion exhibited low, intermediate and high levels of calretinin or calbindin staining without any discernible spatial organization, while anti-β-tubulin antibody staining levels of these neurons were largely uniform (Fig. 3B-E, G-J). Notably, when neurons in different tonotopic regions were compared in the low magnification image, overall level of anti-calretinin staining irradiance in the mid-cochlea appeared to be higher than that of the very basal region (Fig. 3A). Anti-calbindin staining levels also showed a slightly decreasing trend from the middle to the base, but only very limited difference was observed (Fig. 3F).

In order to examine the distribution of the two calcium binding proteins we co-labeled acutely prepared cochlear whole-mounts with anti-calretinin and anti-calbindin antibodies (Fig. 4A and 4B, respectively). We found that the heterogeneous distribution patterns of each calcium binding protein labeling showed varying degrees of overlap. While the majority of neurons possessed relatively low levels of both proteins with a continuum of combinations (Fig. 4A-C, arrow), high levels of calretinin (red) and calbindin (green) staining irradiance were mainly present in distinct, non-overlapping subpopulations of cells (Fig. 4A-C, arrowheads). Neurons labeled with high levels of both calcium binding proteins were relatively rare (Fig. 4A-C, asterisk). This pattern was quantitated from an *in vitro* neuronal culture system which showed essentially identical staining patterns (Fig. 4D) and provided the opportunity to evaluate electrophysiological firing patterns.

Calretinin and calbindin distributions were quantified from immunostained images, normalized, and plotted in frequency histograms (Figs. 4E and 4F, respectively). Each was well fitted with the sum of three Gaussians, yet with distinct means (calretinin: 0.10, 0.22, 0.42 and calbindin: 0.08, 0.15, 0.24). When the irradiance values for calretinin were plotted against calbindin from each location (Fig. 4G) the data confirmed our observations that the majority of cells exhibited low levels of calretinin and calbindin staining irradiance (category III in Fig. 4G and inset; n=148) and that the high calretinin (category IV, n=74) and calbindin (category II, n=87) staining irradiance was relatively non-overlapping since only 11 neurons were observed in category I. Thus, the intracellular distribution of calretinin and calbindin distribution mainly fell into three broad categories in which either calretinin or calbindin irradiance predominated or there was relatively low levels of both calcium binding proteins.

Tonotopic variation of calretinin and calbindin staining levels *in vitro*

The spiral ganglion exhibits a tonotopic gradient of neuronal firing patterns, neurotrophin levels, voltage-gated ion channel density, and synaptic protein distribution (Davis, 2003; Flores-Otero et al., 2007). It has also been shown that calbindin levels in hair cells vary with tonotopic position in both mammalian (Pack and Slepecky, 1995) and chick cochlea (Hiel et al., 2002). To determine whether the heterogeneous distribution of calretinin and calbindin in mouse spiral ganglion is also related to tonotopic organization, we compared quantitative staining irradiance measurements of calretinin and calbindin in three separate frequency regions.

For calretinin, the heterogeneity is present in each of the tonotopic locations that we evaluated (Fig. 5A-C) in contrast to a relatively uniform neuronal β-tubulin staining pattern (Fig. 5D-F). This local heterogeneous pattern was quantified by histograms of normalized staining irradiance measurements in each tonotopic region pooled from seven individual experiments (Fig. 5G-I, dark bars). Histograms constructed from the staining measurements of base, middle and apex neurons in all seven individual experiments could be best fitted with the sum (Fig. 5G-I, purple fitted curves) of three Gaussians (Fig. 5G-I, yellow, cyan and pink fitted curves) with distinct means (base: 0.064, 0.174, 0.428; middle: 0.097, 0.220, 0.407; apex: 0.043, 0.125, 0.251), indicating the presence of multiple populations with differential staining levels in each region. This heterogeneity could also be observed in histograms of data from a single experiment as a subset of the group data (Fig. 5G-I, light bars), which did not capture the full extent of complexity due to the necessarily limited number of observations (100~200 for each region). Interestingly, we found that the average calretinin staining irradiance for individual experiments was significantly higher in the middle region (0.214±0.011) compared with the base (0.139±0.011) and apex (0.134±0.015) regions (n=7, $p<0.01$, Fig. 5J). This quantitative result was also consistent with our qualitative observation in the paraffin embedded sections as described above (Fig 3A).

Calbindin staining irradiance, similar to calretinin, was heterogeneously distributed in neuronal cultures from all tonotopic regions (Fig. 6A-F) with different fitted Gaussian mean values (base: 0.110, 0.187, 0.364; middle: 0.132, 0.276, 0.477; apex: 0.121, 0.251, 0.379, Fig. 6G-I). However, in contrast to the calretinin staining pattern, average calbindin staining irradiance in cultured neurons did not display significant difference within different tonotopic location (base, 0.233±0.024; middle, 0.236±0.018; apex, 0.234±0.020, n=7, $F(2,18)= 0.0027$, Fig. 6J).

In summary, the heterogeneous staining patterns of anti-calretinin and anti-calbindin antibodies were not attributable to tonotopy since they were observed throughout the apical, middle and basal regions. Nevertheless, we did find that the immunostaining levels for one of the calcium binding proteins, calretinin, was significantly higher overall in the mid-cochlear region, while calbindin exhibited comparable staining irradiance in all regions.

Calretinin and calbindin staining levels and neuronal intrinsic firing properties

The role of calretinin and calbindin as calcium buffers that regulate intracellular calcium levels and neuronal excitability has been well characterized (Schwaller et al., 2002). The

non-linear calretinin distribution within the ganglion opened up the possibly that it might reflect the enhancement of synaptic transmission in the mid-cochlear region (Meyer et al., 2009) or, alternatively, correlate with the higher overall threshold sensitivity of some neurons in the mid-cochlea within a population displaying significant threshold heterogeneity (Liu and Davis, 2007). In order to directly assess whether levels of calretinin and calbindin are correlated with and potentially responsible for these observations, we took advantage of the accessibility of our *in vitro* neuronal culture and related the calretinin and calbindin staining profiles to electrophysiological features. Recordings were made from *in vitro* neuronal cultures isolated from basal, middle and apical regions of the spiral ganglion. To accurately measure excitability and kinetics parameters, we determined the resting membrane potential using the previously described non-invasive method (Verheugen et al., 1999) and measured the voltage threshold, action potential latency, duration and time constant in whole-cell current clamp mode. Differential voltage, defined as the difference between holding potential and the voltage threshold, was also calculated to probe the intrinsic excitability of each neuron. A total of 88 recordings were used for subsequent analysis (base n=32, middle n=31, apex n=25).

First we established that when held at their endogenous resting membrane potentials, the population of spiral ganglion neurons used for the study exhibited the full range of heterogeneous and tonotopically-related firing patterns observed previously (Adamson et al., 2002; Liu and Davis, 2007). As expected, we found that in base, middle and apex (Fig. 7A-C), the maximum number of spikes a neuron could fire (AP_{max}) increased from base to apex (base 2.72±0.82, middle 10.74±1.77, apex 14.24±1.92; Fig. 7D, black bars). Furthermore, consistent with previous findings, both intrinsic excitability and firing kinetics were heterogeneous in each region and were generally graded along the tonotopic axis. Onset time constant (base 3.48±0.20ms, middle 6.81±0.66ms, apex 9.13±0.91ms, $p<0.01$ for base and middle, base and apex; $p<0.05$ for middle and apex; Fig. 7E, black bars), action potential latency (base 6.39±0.23ms, middle 9.20±0.42ms, apex 11.59±0.90ms, $p<0.01$ for all pairwise comparisons) and action potential duration (base 1.07±0.03ms, middle 1.11±0.03ms, apex 1.18±0.04ms, base and apex, $p<0.05$) all showed tonotopic trends that increased from base to apex. In contrast to this, and in accord with previous findings (Liu and Davis, 2007), excitability-related parameters showed non-linear trends such that resting membrane potential, voltage threshold and differential voltage (Fig. 7F, black bars) were comparable in the middle and the apex (resting membrane potential: middle −64.86±0.31mV, apex −64.90±0.41mV; voltage threshold: middle −45.30±0.62mV, apex −44.98±0.95mV; differential voltage: middle 19.48±0.66mV, apex 20.00±1.07mV) but neurons from the base displayed significantly ($p<0.01$) lower resting membrane potential (−66.74±0.38mV), higher voltage threshold (−41.07±0.65mV) and higher differential voltage (25.74±0.82mV).

To correlate calretinin/calbindin content with electrophysiological phenotype, patch-clamp recordings were made from neurons that were subsequently examined with immunocytochemistry. The characteristics of these neurons (base n=15, middle n=12, apex n=13) were representative of the overall electrophysiological patterns (Fig. 7D-F, gray bars) and calcium binding protein staining profiles (Fig. 8F-G), described above, thus

incorporating the full complexity of phenotypes within the ganglion. Comparisons were made with normalized fluorescence intensity; however, non-normalized irradiance levels showed similar results. Of the parameters examined, none correlated with individual comparisons of either calretinin or calbindin staining irradiance levels (Fig. 8A-B. R^2 of each parameter with calretinin or calbindin, respectively: time constant, 0.008 and 0.008; differential voltage, 0.071 and 0.041; latency, 0.002 and 0.015; duration, 0.058 and 0.006; AP max, 0.022 and 0.050; resting membrane potential, 0.017 and 0.038; voltage threshold, 0.067 and 0.019). Representative examples of two parameters, differential voltage and onset tau, which represent excitability- and timing-related parameters, are shown in Figure 8A and 8B, respectively.

Interestingly, however, when we utilized the calbindin/calretinin ratio rather than simple levels of individual factors, a striking correlation with electrophysiological properties did emerge (Fig. 8D). For the action potential onset tau, neurons with slow kinetics showed normalized calbindin/calretinin staining irradiance ratio values scattered around 1.0 with relatively small deviation. This was quite unlike the calbindin/calretinin staining irradiance ratio values for fast onset neurons which showed a much wider diversity of labeling patterns. A quantitative comparison between slow onset neurons (onset tau > 7.0 ms) and that of the fast onset neurons (onset tau < 7.0 ms) showed distinct distributions (Kolmogorov-Smirnov test, $p<0.05$), indicating that spiral ganglion neurons with slow-kinetics possess comparable relative levels of calbindin and calretinin proteins, while the relative levels of calretinin and calbindin in neurons with fast-kinetics vary within a broader range (Figure 8E). Of the electrophysiological parameters that we examined, latency, another parameter that is closely related to onset tau, showed a similar but less organized pattern. The other parameters unrelated to the firing kinetics did not show an obvious correlation with the calbindin/ calretinin ratio (e.g. Fig. 8C).

Heterogeneity of anti-calretinin and anti-calbindin staining in type II neurons

While calretinin and calbindin do not appear to regulate intrinsic firing properties of spiral ganglion neurons directly, the complexity of the spiral ganglion revealed by their differential distribution patterns may be associated with other aspects of functional diversity. Thus, similar to the calretinin and calbindin co-labeling pattern in the retina that indicates separate parallel pathways demarked by calcium binding protein distribution (Mojumder et al., 2008), we wondered whether this was also the case in the spiral ganglion. To explore this possibility further, we took advantage of the type II neuron marker peripherin (Hafidi, 1998) , which has been previously validated to stain type II spiral ganglion neurons specifically (Mou et al., 1998). Co-labeling of peripherin with either calretinin or calbindin was characterized in individual experiments to obtain unequivocal profiles calretinin and calbindin distributions in type I and type II neurons *in vitro.*

Putative type II neurons strongly labeled by anti-peripherin antibody exhibited low levels of calretinin staining *in vitro* (Fig. 9A-D), a finding consistent with our observations in acute preparations (data not shown). Pooled data from the seven experiments previously examined (Fig. 5) showed that even after putative type II neurons were removed from the analysis they retained their heterogeneous pattern and could still be fitted with the sum of three Gaussians

(mean 0.071, 0.178, 0.343). The putative type II neurons, overall, had lower anti-calretinin staining levels (Fig. 9E), which were best fitted by a single Gaussian with relatively low mean value (0.036). When the average calretinin staining irradiance of putative type I and putative type II neurons obtained from seven individual experiments were compared, putative type I neurons showed a significantly higher value than the type II neurons (type I, 0.171±0.010; type II, 0.091±0.015; n=7, $p<0.01$, Fig. 9F).

In order to determine whether the total results reflected the staining patterns in all or a subset of type II spiral ganglion neurons we made systematic comparisons between different tonotopic regions (Fig. 9G). From our observations of individual experiments, an example of which is shown in figure 9G, we noted that a preponderance of the putative type II neurons with the lowest anti-calretinin labeling were from the apex (Fig. 9G, red symbols). This observation is also seen in the group data from seven experiments analyzed by tonotopic location (Fig. 9H). Type I neurons consistently showed the same trend as the overall data, such that the highest average calretinin levels appeared in the middle. Type II neurons, although with the expected fewer numbers of neurons, displayed significantly lower calretinin levels in the apex ($p<0.05$). Taken together, it appears that the greatest difference between type I and type II neurons was manifested in the apical region, thus, revealing a sub-class of type II neurons when evaluated for anti-calretinin immunolabeling.

The relationship between neuronal classes described above is reversed for calbindin-containing putative type II neurons. In this case we noted that peripherin-stained neurons co-labeled with anti-calbindin antibody (Fig. 10A-D), while showing an overall broad range of intensity levels (Fig. 10E) the average of which was significantly higher than putative type I neurons (Fig. 10F) due to the higher levels in apical type II neurons (Fig. 10G, red symbols). Average data from seven experiments analyzed from different tonotopic regions (Fig. 10G) showed that while the average calbindin staining irradiance for type I neurons remained comparable in all tonotopic locations (base 0.235±0.025, n=7; middle 0.235±0.017, n=7; apex 0.211±0.021, n=7) and for the base and middle type II neurons (0.200±0.031, n=7 and 0.258±0.065, n=5, respectively), only the apical type II neurons were significantly higher in their anti-calbindin staining irradiance (0.390±0.024, n=7; $p<0.05$). Thus, similar to calretinin, differences between type I and type II calbindin staining levels were only statistically significant in the apex, reaffirming that based on calcium binding protein levels the apical type II neurons have a distinct phenotype.

Discussion

Although the presence and abundance of calcium binding proteins in specific cell types is routinely utilized as a cell-type marker (DeFelipe et al., 1999; Markram et al., 2004), only when it has been found to be causal for a specific firing pattern has their functional significance been unequivocally identified within a particular class of neurons (Klapstein et al., 1998; Gall et al., 2003). We noted that antibodies against the calcium binding proteins calretinin and calbindin showed clear categories of low, medium, and high immunolabeling in the spiral ganglion and, thus, herein sought to determine the significance of this observation. We recognized that because the spiral ganglion is composed predominately of a single class of cells, 95% of which are classified as type I spiral ganglion neurons based on

their one-to-one innervation of inner hair cells (Ryugo, 1992), one might hypothesize that the obviously different staining levels would most likely correspond to functional, rather than cellular markers. Thus, by studying the neurons within a system in which the electrophysiological profile has been documented, a direct exploration can be made of whether endogenous firing patterns are related to the abundance of calretinin and/or calbindin. Furthermore, because the location of neurons along two dimensions of the cochlear axis has significance for sensory coding (frequency along the cochlear axis, intensity orthogonal to the tonotopic map), the distribution of a protein, should it correspond to one or both of these patterns, would help to unravel its functional significance. Therefore, the spiral ganglion provides an ideal opportunity to explore the neuron-specific role of calcium binding proteins and, in turn, documenting the distribution of calcium binding proteins in these cells could also reveal more about the neurons within this seemingly simple peripheral sensory ganglion.

Taking this approach, we determined that there is an intricate pattern of calcium binding protein labeling superimposed on the known distributions of intrinsic electrophysiological properties (Adamson et al., 2002; Liu and Davis, 2007) and synaptic protein distributions (Flores-Otero et al., 2007; Flores-Otero and Davis, 2011). Overall, different levels of anti-calretinin and anti-calbindin labeling are documented within each region of the cochlea for type I spiral ganglion neurons, showing that calretinin levels were significantly higher in the middle while calbindin levels were relatively uniform across different regions. Surprisingly, we also noted that type II spiral ganglion neurons isolated from the apex with their distinct calcium binding protein profile having high calbindin and little to no calretinin, differed from type II neurons in the mid and basal regions. These observations indicate that within both classes of spiral ganglion neuron there resides additional dimensions of complexity revealed by their calretinin and calbindin levels, which adds to the rich diversity displayed by postnatal spiral ganglion neurons.

Calretinin and calbindin levels and intrinsic firing features

Both gain-of-function and lost-of-function studies have demonstrated the important roles that calretinin and calbindin have in shaping action potential parameters. For example, in the cerebellum, it was shown in knockout animals that endogenous calretinin elongates the duration of action potentials and decreases the rate of sustained firing (Gall et al., 2003). Conversely, calbindin in hippocampal neurons attenuates the rapid afterhyperpolarization and reduces adaption of firing (Klapstein et al., 1998). Therefore, although the two calcium binding proteins have very similar structure and calcium binding kinetics (Cheung et al., 1993; Nägerl et al., 2000; Faas and Mody, 2012), they may play differential or even opposite roles in a neuron. If the same principles hold true for neurons within the spiral ganglion, one might expect that calretinin levels would be higher in the fast-accommodating basal neurons whereas calbindin would be higher in the slowly-accommodating apical neurons. Yet this was unequivocally not what we observed. Instead we found that calretinin staining levels were higher in the mid-cochlea region, which is also the most behaviorally sensitive region in the spiral ganglion. This finding suggested that levels of calretinin and calbindin were unlikely to be associated with firing accommodation of spiral ganglion neurons, but

immediately raised the question of whether calretinin or calbindin levels were directly related to the intrinsic excitability.

To address this question, we compared the endogenous firing features and the levels of calretinin and calbindin in the same cell. Taking advantage of an established *in vitro* culture system that enabled the combination of electrophysiological recordings with immunocytochemical staining and analysis, we showed that staining levels of calretinin and calbindin alone were not correlated with excitability parameters such as resting membrane potential and firing threshold. Furthermore, no associations were noted between the two calcium binding proteins and kinetic features of neuronal firing, such as action potential duration, time constant, latency and APmax. We did, however, find that the ratio of normalized calbindin staining irradiance to normalized calretinin staining irradiance showed a recognizable pattern that neurons with comparable relative levels of calretinin and calbindin tended to have longer time constants, while the calbindin/calretinin ratio of short-time constant neurons spanned a broader range. Therefore, the relative staining levels of calretinin and calbindin, but not their staining levels alone, may help distinguish slow-kinetics neurons from the fast-kinetics neurons in the spiral ganglion.

In the vestibular ganglion of the inner ear, calretinin and peripherin marked calyx-only and bouton-only afferent terminals and corresponding cell bodies, respectively, while calbindin labeled bouton-only and bimorph afferents (Leonard and Kevetter, 2002; Kevetter, 2002). Interestingly, a recent study showed that although calretinin labeled calyx-only fibers which are believed to be irreglular-firing and have a transient firing response to current steps, the protein itself may not be involved in the regulation of endogenous firing patterns of these neurons. Firing patterns of vestibular ganglion neurons of calretinin knockout mice showed no clear difference with that of wild type mice (Li and Eatock, 2013). Given the distribution of both calretinin and calbindin proteins in the spiral ganglion, we have taken the approach of directly assessing the relation between endogenous firing features and the levels of calretinin and calbindin in wild type tissues, nevertheless, our findings are consistent with the results in the vestibular system, indicating that in the inner ear, levels of either calretinin or calbindin alone in primary neurons is unlikely to be directly associated with categories of intrinsic firing features.

It is known that the average time constant of spiral ganglion neurons increases from base to the apex (Liu and Davis, 2007). Consistent with this, 9 out of 12 neurons in the slow category, which exhibited longer time constants and comparable relative calbindin/calretinin staining levels, were obtained from the apical region. Although it was not possible to examine the identity of the neurons in these experiments with peripherin labeling due to the experimental protocol to stain both calcium binding proteins, it is interesting to ask how the calbindin/calretinin ratio correlates with the difference between type I and type II neurons since the slow-kinetics neurons make up a relatively small population. Nevertheless, because the neurons within this category possess comparable calretinin and calbindin levels, and clearly distinct from the high calbindin and low-calretinin profile of apical type II neurons that resulted in a relatively high calbindin/calretinin ratio, we surmise that it is unlikely that the subpopulation of slow time constant neurons could be solely attributed to type II neurons. Thus, the relationship between the calbindin/calretinin ratio and onset tau of a

neuron may reflect heterogeneity amongst type I as well as type II neurons in all tonotopic regions.

Tonotopic variation of type II neurons

In this study, we have shown that type II neurons in the apex of the spiral ganglion possessed higher levels of calbindin and lower levels of calretinin than type II neurons from the middle and base. This observation is consistent with the distinctive nature of apical type II neurons which differ from type II neurons in other regions in the cochlea. For example, the peripheral fibers of apical type II neurons turn both apically and basally when they reach the outer hair cell region and form synapses with both outer hair cells and support cells, while type II afferents in the middle and base region consistently turn towards the base and connect only with outer hair cells (Burgess et al., 1997; Fechner et al., 2001; Nayagam et al., 2011). Furthermore, the intrinsic properties of type II neurons in cultures prepared from isolated regions of the spiral ganglion showed that type II neurons were not all identical. The apical type II neurons exhibited firing features with faster kinetics and higher firing threshold than basal type II neurons (Reid et al., 2004). Taken together, the distribution patterns of calretinin and calbindin highlighted another aspect of the tonotopic difference among type II neurons, further indicating that type II neurons may also possess specific features that may enable this relatively small population to convey complex sensory information to higher centers.

Local heterogeneity superimposed on tonotopic and intensity map

In addition to the well-known tonotopic specializations within the cochlear duct, the spiral ganglion possesses another orthogonal dimension of spatial organization consistent with the parameters required to build an intensity map. In the cat, neuronal cell bodies of auditory nerves with different spontaneous rates showed a topographic organization in the spiral ganglion such that low and medium spontaneous rate neurons tended to cluster in the scala vestibuli side, and high spontaneous rate neurons were more likely to reside in the scala tympani side (Leake and Synder, 1989; Leake et al., 1992). Because the endogenous features of voltage threshold and resting membrane potential that contribute to neuronal excitability might logically contribute to intensity coding, we reasoned that the lack of a clear correlation between neuron excitability and calcium binding protein irradiance levels would make it unlikely that calretinin or calbindin would be distributed systematically along the scala tympani-vestibuli axis. This is what we found, which is consistent with the idea that calretinin and calbindin levels do not relate to the distinctive categories of spontaneous rate displayed by spiral ganglion neurons (Liberman, 1978; Taberner and Liberman, 2009).

The presynaptic protein, synaptophysin, was previously shown to be graded in both tonotopic and scala vestibuli to scala tympani axes, such that an orthogonal scala vestibuli to scala tympani gradient was superimposed on the average levels of anti-synaptophysin staining irradiance that increased from base to apex (Flores-Otero and Davis, 2011). Therefore, in a restricted tonotopic region, the level of synaptophysin may correlate with the location of neuronal cell body in the ganglion, and, thus, with spontaneous rates of the auditory nerve. To further confirm that levels of calretinin or calbindin were not associated with spontaneous rate of the auditory nerve in mouse cochlea, we also examined the spatial

organization of anti-calretinin and anti-calbindin antibody staining irradiance and their co-labeling patterns with anti-synaptophysin antibody staining. Co-labeling of either calretinin or calbindin antibodies with synaptophysin antibody in neuronal cultures, expectedly, did not reveal any association of staining levels (data not shown). Therefore, both our electrophysiological and immunocytochemical results indicate that neither calretinin nor calbindin levels are associated with spontaneous rate in the murine spiral ganglion.

Although we have shown that the local heterogeneity revealed by anti-calretinin and anti-calbindin staining patterns of calretinin and calbindin could not be related to the known intensity map, it remains possible that calretinin and calbindin could associate with other functional features or differentially regulate electrophysiological events beyond membrane responses at neuronal cell soma. There is growing evidence that spiral ganglion neurons are heterogeneous in terms of their protein profile (Romand et al., 1990; Järlebark et al., 2000; Khan et al., 2002; Khalifa et al., 2003; Inoue et al., 2006), and that type I and type II neurons could possess distinct distribution patterns of proteins crucial to the membrane properties, such as Na/K ATPase and sodium channels (McLean et al., 2009; Fryatt et al., 2009). In this context, the distribution of calretinin and calbindin may be related to, or be indicative of, a repertoire of functional differences within the spiral ganglion independent of the known tonotopic and intensity maps.

For example, in addition to their direct role of shaping neuronal firing in cerebellar granular cells and hippocampal neurons, as described above, calretinin and calbindin are also involved in indirect regulation of cellular function. Loss of calretinin impairs synaptic plasticity in dentate gyrus without affecting basal synaptic transmission (Schurmans et al., 1997), and tissue specific calbindin overexpression in the same region leads to an increase of presynaptic strength and reduction of long-term potentiation (Dumas et al., 2004). The central projections of spiral ganglion neurons form connections with highly diverse targets in the cochlear nucleus, and the morphological features of their fiber endings could vary independent of their characteristic frequency and spontaneous rate (Liberman, 1991; Rouiller et al., 1986; Ryugo and Rouiller, 1988; Ryugo, 1992).

In summary, this study suggests that different levels of calretinin and calbindin do correlate with specific subpopulation of cells, and may lead to a better understanding of the functions in apical type II neurons in particular. Moreover, the door is still open for an association with the heterogeneity of intrinsic and synaptic properties among spiral ganglion neurons, and our findings may help to reveal a novel dimension of complexity that may serve as the cellular basis for additional neuronal processing in the primary auditory nerve.

Supplementary Material

Refer to Web version on PubMed Central for supplementary material.

Acknowledgments

We would like to thank Dr. Mark R. Plummer and Dr. Robert Crosier for critical reading of previous versions of the manuscript, Huizhong Xue for technical support with animal dissection and culture preparation, Dr Noriko Kane-Goldsmith and the Neuroscience Imaging Facility at W.M. Keck Center for Collaborative Neuroscience, Rutgers University, for assistance with confocal imaging.

Grant information:

The work is supported by NIH NIDCD RO1 DC01856

Reference

Adamson CL, Reid MA, Mo Z-L, Bowne-English J, Davis RL. Firing features and potassium channel content of murine spiral ganglion neurons vary with cochlear location. J Comp Neurol. 2002; 447:331–350. [PubMed: 11992520]

Airaksinen MS, Eilers J, Garaschuk O, Thoenen H, Konnerth A, Meyer M. Ataxia and altered dendritic calcium signaling in mice carrying a targeted null mutation of the calbindin D28k gene. Proc Natl Acad Sci U S A. 1997; 94:1488–1493. [PubMed: 9037080]

Angelo K, Rancz EA, Pimentel D, Hundahl C, Hannibal J, Fleischmann A, Pichler B, Margrie TW. A biophysical signature of network affiliation and sensory processing in mitral cells. Nature. 2012; 488:375–378. [PubMed: 22820253]

Baizer JS, Broussard DM. Expression of calcium-binding proteins and nNOS in the human vestibular and precerebellar brainstem. J Comp Neurol. 2010; 518:872–895. [PubMed: 20058225]

Bizley JK, Walker KMM. Sensitivity and selectivity of neurons in auditory cortex to the pitch, timbre, and location of sounds. Neuroscientist. 2010; 16:453–469. [PubMed: 20530254]

Brown MC. Antidromic responses of single units from the spiral ganglion. J Neurophysiol. 1994; 71:1835–1847. [PubMed: 8064351]

Burgess BJ, Adams JC, Nadol JB. Morphologic evidence for innervation of Deiters' and Hensen's cells in the guinea pig. Hear Res. 1997; 108:74–82. [PubMed: 9213124]

Cheung WT, Richards DE, Rogers JH. Calcium binding by chick calretinin and rat calbindin D28k synthesised in bacteria. Eur J Biochem. 1993; 215:401–410. [PubMed: 8344307]

Davis RL. Gradients of Neurotrophins, Ion Channels, and Tuning in the Cochlea. Neuroscientist. 2003; 9:311–316. [PubMed: 14580116]

Dechesne CJ, Rabejac D, Desmadryl G. Development of calretinin immunoreactivity in the mouse inner ear. J Comp Neurol. 1994; 346:517–529. [PubMed: 7983242]

Dechesne CJ, Thomasset M. Calbindin (CaBP 28kDa) appearance and distribution during development of the mouse inner ear. J Comp Neurol. 1988; 40:233–242.

DeFelipe J, González-Albo MC, Del Río MR, Elston GN. Distribution and patterns of connectivity of interneurons containing calbindin, calretinin, and parvalbumin in visual areas of the occipital and temporal lobes of the macaque monkey. J Comp Neurol. 1999; 412:515–526. [PubMed: 10441237]

DeFelipe J. Types of neurons, synaptic connections and chemical characteristics of cells immunoreactive for calbindin-D28K, parvalbumin and calretininin the neocortex. J Chem Neuroanat. 1997; 14:1–19. [PubMed: 9498163]

Dhawale AK, Hagiwara A, Bhalla US, Murthy VN, Albeanu DF. Non-redundant odor coding by sister mitral cells revealed by light addressable glomeruli in the mouse. Nat Neurosci. 2010; 13:1404–1412. [PubMed: 20953197]

Dumas TC, Powers EC, Tarapore PE, Sapolsky RM. Overexpression of calbindin D(28k) in dentate gyrus granule cells alters mossy fiber presynaptic function and impairs hippocampal-dependent memory. Hippocampus. 2004; 14:701–709. [PubMed: 15318329]

Faas GC, Mody I. Measuring the kinetics of calcium binding proteins with flash photolysis. Biochim Biophys Acta. 2012; 1820:1195–1204. [PubMed: 22001612]

Fechner FP, Nadol JBJR, Burgess BJ, Brown MC. Innervation of supporting cells in the apical turns of the guinea pig cochlea is from type II afferent fibers. J Comp Neurol. 2001; 429:289–298. [PubMed: 11116221]

Field GD, Chichilnisky EJ. Information processing in the primate retina: circuitry and coding. Annu Rev Neurosci. 2007; 30:1–30. [PubMed: 17335403]

Flores-Otero J, Davis RL. Synaptic proteins are tonotopically graded in postnatal and adult type I and type II spiral ganglion neurons. J Comp Neurol. 2011; 519:1455–1475. [PubMed: 21452215]

Flores-Otero J, Xue HZ, Davis RL. Reciprocal regulation of presynaptic and postsynaptic proteins in bipolar spiral ganglion neurons by neurotrophins. J Neurosci. 2007; 27:14023–14034. [PubMed: 18094241]

Fryatt AG, Vial C, Mulheran M, Gunthorpe MJ, Grubb BD. Voltage-gated sodium channel expression in rat spiral ganglion neurons. Mol Cell Neurosci. 2009; 42:399–407. [PubMed: 19765660]

Fuentes-Santamaria V, Alvarado JC, Taylor AR, Brunso-Bechtold JK, Henkel CK. Quantitative changes in calretinin immunostaining in the cochlear nuclei after unilateral cochlear removal in young ferrets. J Comp Neurol. 2005; 483:458–475. [PubMed: 15700274]

Gall D, Roussel C, Susa I, D'Angelo E, Rossi P, Bearzatto B, Galas MC, Blum D, Schurmans S, Schiffmann SN. Altered neuronal excitability in cerebellar granule cells of mice lacking calretinin. J Neurosci. 2003; 23:9320–9327. [PubMed: 14561859]

Gollisch T, Meister M. Eye smarter than scientists believed: neural computations in circuits of the retina. Neuron. 2010; 65:150–164. [PubMed: 20152123]

Hafidi A. Peripherin-like immunoreactivity in type II spiral ganglion cell body and projections. Brain Res. 1998; 805:181–190. [PubMed: 9733963]

Haverkamp S, Wässle H. Immunocytochemical Analysis of the Mouse Retina. J Comp Neurol. 2000; 424:1–23. [PubMed: 10888735]

Hiel H, Navaratnam DS, Oberholtzer JC, Fuchs P a. Topological and Developmental Gradients of Calbindin Expression in the Chick's Inner Ear. J Assoc Res Otolaryngol. 2002; 3:1–15. [PubMed: 12083720]

Huang L-C, Thorne PR, Housley GD, Montgomery JM. Spatiotemporal definition of neurite outgrowth, refinement and retraction in the developing mouse cochlea. Development. 2007; 134:2925–2933. [PubMed: 17626062]

Inoue T, Matsubara A, Maruya S, Yamamoto Y, Namba A, Sasaki A, Shinkawa H. Localization of dopamine receptor subtypes in the rat spiral ganglion. Neurosci Lett. 2006; 399:226–229. [PubMed: 16490310]

Järlebark LE, Housley GD, Thorne PR. Immunohistochemical localization of adenosine 5'-triphosphate-gated ion channel P2X(2) receptor subunits in adult and developing rat cochlea. J Comp Neurol. 2000; 421:289–301. [PubMed: 10813788]

Keithley EM, Schreiber RC. Frequency map of the spiral ganglion in the cat. J Acoust Soc Am. 1987; 81:1036–1042. [PubMed: 3571719]

Kevetter G. Molecular probes of the vestibular nerve II. Characterization of neurons in Scarpa's ganglion to determine separate populations within the nerve. Brain Res. 2002; 928:18–29. [PubMed: 11844468]

Khalifa SAM, Friberg U, Illing RB, Rask-Andersen H. Synaptophysin immunohistochemistry in the human cochlea. Hear Res. 2003; 185:35–42. [PubMed: 14599690]

Khan KM, Drescher MJ, Hatfield JS, Khan A-M, Drescher DG. Muscarinic receptor subtypes are differentially distributed in the rat cochlea. Neuroscience. 2002; 111:291–302. [PubMed: 11983315]

Klapstein GJ, Vietla S, Lieberman DN, Gray P a, Airaksinen MS, Thoenen H, Meyer M, Mody I. Calbindin-D28k fails to protect hippocampal neurons against ischemia in spite of its cytoplasmic calcium buffering properties: evidence from calbindin-D28k knockout mice. Neuroscience. 1998; 85:361–373. [PubMed: 9622236]

Leake PA, Snyder RL, Merzenich MM. Topographic organization of the cochlear spiral ganglion demonstrated by restricted lesions of the anteroventral cochlear nucleus. J Comp Neurol. 1992; 320:468–478. [PubMed: 1629399]

Leake PA, Synder RL. Topographic organization of the central projections of the spiral ganglion in cats. J Comp Neurol. 1989; 281:612–629. [PubMed: 2708585]

Leinwand SG, Chalasani SH. Olfactory networks: from sensation to perception. Curr Opin Genet Dev. 2011; 21:806–811. [PubMed: 21889328]

Leonard RB, Kevetter GA. Molecular probes of the vestibular nerve. I. Peripheral termination patterns of calretinin, calbindin and peripherin containing fibers. Brain Res. 2002; 928:8–17. [PubMed: 11844467]

Li GQ, Eatock RA. A constitutive null mutation for calretinin has no effect on excitability of vestibular ganglion neurons. Abstracts of the 36th Annual Midwinter meeting of the Association of Research for Otolaryngology. 2013:117.

Liberman MC. Auditory-nerve response from cats raised in a low-noise chamber. J Acoust Soc Am. 1978; 63:442–55. [PubMed: 670542]

Liberman MC. Single-neuron labeling in the cat auditory nerve. Science. 1982; 216:1239–1240. [PubMed: 7079757]

Liberman MC. Central projections of auditory-nerve fibers of differing spontaneous rate. I. Anteroventral cochlear nucleus. J Comp Neurol. 1991; 313:240–258. [PubMed: 1722487]

Liu Q, Davis RL. Regional specification of threshold sensitivity and response time in CBA/CaJ mouse spiral ganglion neurons. J Neurophysiol. 2007; 98:2215–2222. [PubMed: 17715200]

Ma Q. Population coding of somatic sensations. Neurosci bull. 2012; 28:91–99. [PubMed: 22466120]

Markram H, Toledo-Rodriguez M, Wang Y, Gupta A, Silberberg G, Wu C. Interneurons of the neocortical inhibitory system. Nat Rev Neurosci. 2004; 5:793–807. [PubMed: 15378039]

Marmigère F, Ernfors P. Specification and connectivity of neuronal subtypes in the sensory lineage. Nat Rev Neurosci. 2007; 8:114–127. [PubMed: 17237804]

McLean WJ, Smith KA, Glowatzki E, Pyott SJ. Distribution of the Na,K-ATPase alpha subunit in the rat spiral ganglion and organ of corti. J Assoc Res Otolaryngol. 2009; 10:37–49. [PubMed: 19082858]

Meyer AC, Frank T, Khimich D, Hoch G, Riedel D, Chapochnikov NM, Yarin YM, Harke B, Hell SW, Egner A, et al. Tuning of synapse number, structure and function in the cochlea. Nat Neurosci. 2009; 12:444–453. [PubMed: 19270686]

Mo Z, li; Davis, RL. Endogenous Firing Patterns of Murine Spiral Ganglion Neurons. J Neurophysiol. 1997:1294–1305. [PubMed: 9084597]

Mojumder DK, Wensel TG, Frishman LJ. Subcellular compartmentalization of two calcium binding proteins, calretinin and calbindin-28 kDa, in ganglion and amacrine cells of the rat retina. Mol Vis. 2008; 14:1600–1613. [PubMed: 18769561]

Mou K, Adamson CL, Davis RL. Time-Dependence and Cell-Type Specificity of Synergistic neurotrophin Actions on Spiral Ganglion Neurons. J Comp Neurol. 1998; 402:129–139. [PubMed: 9831050]

Nägerl UV, Novo D, Mody I, Vergara JL. Binding kinetics of Calbindin-D28k determinedby flash photolysis of caged Ca. Biophys J. 2000; 79:3009–3018. [PubMed: 11106608]

Nayagam BA, Muniak MA, Ryugo DK. The spiral ganglion: connecting the peripheral and central auditory systems. Hear Res. 2011; 278:2–20. [PubMed: 21530629]

Pack AK, Slepecky NB. Cytoskeletal and calcium-binding proteins in themammalian organ of Corti: cell type-specific proteins displaying longitudinal and radial gradients. Hear Res. 1995; 91:119–135. [PubMed: 8647714]

Reed-Geaghan EG, Maricich SM. Peripheral somatosensation: a touch of genetics. Curr Opin Genet Dev. 2011; 21:240–248. [PubMed: 21277195]

Reid MA, Flores-Otero J, Davis RL. Firing patterns of type II spiral ganglion neurons in vitro. J Neurosci. 2004; 24:733–742. [PubMed: 14736859]

Robertson D. Horseradish peroxidase injection of physiologically characterized afferent and efferent neurones in the guinea pig spiral ganglion. Hear Res. 1984; 15:113–121. [PubMed: 6490538]

Romand R, Sobkowicz H, Emmerling M, Whitlon D, Dahl D. Patterns of neurofilament stain in the spiral ganglion of the developing and adult mouse. Hear Res. 1990; 49:119–125. [PubMed: 1705539]

Rouiller EM, Cronin-Schreiber R, Fekete DM, Ryugo DK. The central projections of intracellularly labeled auditory nerve fibers in cats: an analysis of terminal morphology. J Comp Neurol. 1986; 249:261–278. [PubMed: 3734159]

Ruggero, MA. Physiology and coding of sound in the auditory nerve. In: Popper, AN.; Fay, RR., editors. The Mammalian auditory pathway: Neurophysiology. Springer-Verlag; New York: 1992. p. 34-93.

Ryugo DK, Rouiller EM. Central projections of intracellularly labeled auditory nerve fibers in cats: morphometric correlations with physiological properties. J Comp Neurol. 1988; 271:130–142. [PubMed: 3385008]

Ryugo, DK. The auditory nerve: peripheral innervation cell body:morphology. The mammalian auditory pathway: neuroanatomy. In: Popper, AN.; Fay, RR.; Webster, DB., editors. Springer-Verlag; New York: 1992.

Schurmans S, Schiffmann SN, Gurden H, Lemaire M, Lipp HP, Schwam V, Pochet R, Imperato A, Böhme G a, Parmentier M. Impaired long-term potentiation induction in dentate gyrus of calretinin-deficient mice. Proc Natl Acad Sci U S A. 1997; 94:10415–10420. [PubMed: 9294225]

Schwaller B, Meyer M, Schiffmann S. "New" functions for "old" proteins: the role of the calcium-binding proteins calbindin D-28k, calretinin and parvalbumin, in cerebellar physiology. Studies with knockout mice. Cerebellum. 2002; 1:241–258. [PubMed: 12879963]

Schwaller B. The continuing disappearance of "pure" Ca2+ buffers. Cell Mol Life Sci. 2009; 66:275–300. [PubMed: 19099190]

Slepecky, NB. Structure of the mammalian cochlea. In: Dallos, P.; Popper, AN.; Fay, RR., editors. The cochlea. Springer-Verlag; New York: 1996.

Taberner AM, Liberman MC. Response Properties of Single Auditory Nerve Fibers in the Mouse. J Neurophysiol. 2009; 93:557–569. [PubMed: 15456804]

Verheugen, J a; Fricker, D.; Miles, R. Noninvasive measurements of the membrane potential and GABAergic action in hippocampal interneurons. J Neurosci. 1999; 19:2546–2555. [PubMed: 10087068]

Wässle H. Parallel processing in the mammalian retina. Nat Rev Neurosci. 2004; 5:747–757. [PubMed: 15378035]

Weisz C, Glowatzki E, Fuchs P. The postsynaptic function of type II cochlear afferents. Nature. 2009; 461:1126–1129. [PubMed: 19847265]

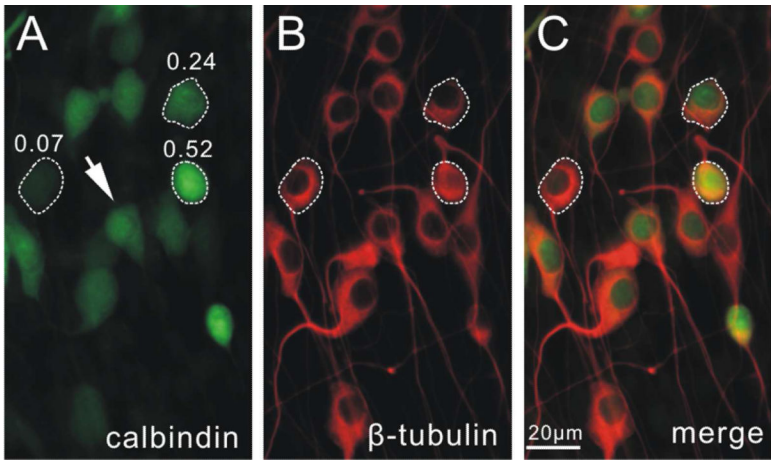

Figure 1. Subcellular distribution and characterization of immunostaining levels

Representative double immune-stained images of neuronal cultures using anti-calbindin (**A**) and anti-β-tubulin (**B**) antibodies. **C**, merged image. Note that calbindin staining was heterogeneous while β-tubulin staining level was relatively uniform in all cells. Arrow, a neuron stained with anti-calbindin antibody showed brighter spots in the nuclei, suggesting differential staining levels within different sub-cellular compartments. Three cells with high, intermediate and low levels were circled with dashed line, and the normalized calbindin staining irradiance values was indicated on top of each cell in A. A magenta-green version of this figure is available as supplementary materials.

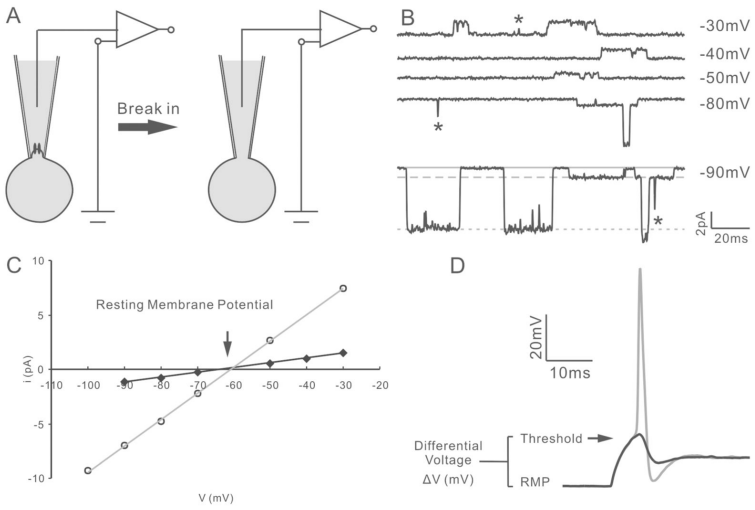

Figure 2. Non-invasive measurement of resting membrane potential

A, diagram of the recording procedure. Cell-attached single channel recording was used to non-invasively assess the resting membrane potential (left). Additional suction was applied to break-in for subsequent whole-cell current clamp recording (right). **B**, single channel traces at the indicated test potentials from −60mV holding potential. Based on relative amplitude, two types of channel openings with small and large amplitudes could be observed. Solid line, closed state; dashed line, opening of the small-conductance channel; dotted line, opening of the large-conductance channel. Transient currents (asterisk) were due to incomplete channel opening events and were not used for the analysis of conductance. **C**, I-V relation of two channels plotted from the recordings in **B**. The two channels exhibited distinctive conductances (43.7pS and 240.6pS) but comparable reversal potentials (−63.5mV and −60.3mV, respectively). **D**, superimposed exemplary traces showing sub-threshold (black) and threshold (gray) measurements of voltage threshold and differential voltage. The cell was held at the endogenous resting membrane potential calculated on-line from cell-attached recording.

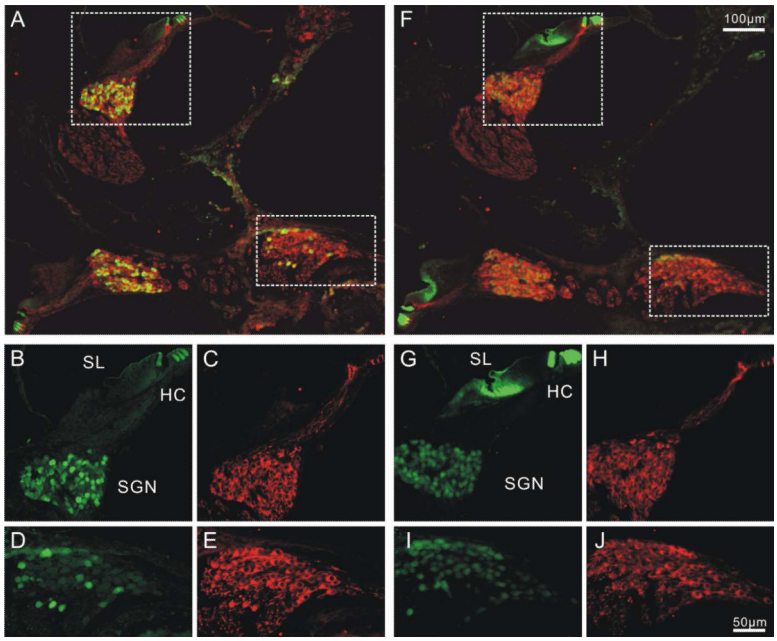

Figure 3. Distribution patterns of calretinin and calbindin in P6 mouse cochlea

Two cochlear sections in close proximity were stained with anti-calretinin (**A-E**) and anti-calbindin antibodies (**F-J**) respectively. Both anti-calretinin and anti-calbindin antibody staining showed heterogeneous patterns in the spiral ganglion. HC, hair cell. SGN, spiral ganglion. SL, spiral limbus. **A**, Low magnification image of cochlear sections double labeled with anti-β-tubulin (red) and anti-calretinin (green) antibodies **B-E,** High magnification images of middle (**B-C**) and basal (**D-E**) neuronal regions enclosed by dotted line in **A**. **F,** low magnification image of a cochlear section showing double labeling of anti-calbindin (green) and anti-β-tubulin (red) antibodies. Prominent calbindin staining was also observed in the spiral limbus **G-J**, High magnification image of the middle (**G, H**) and basal (**I,J**) regions as squared in **F**. Scale bar in **F** applies to **A, F**. Scale bar in **J** applied to **B-E, G-J.** A magenta-green version of this figure is available as supplementary materials.

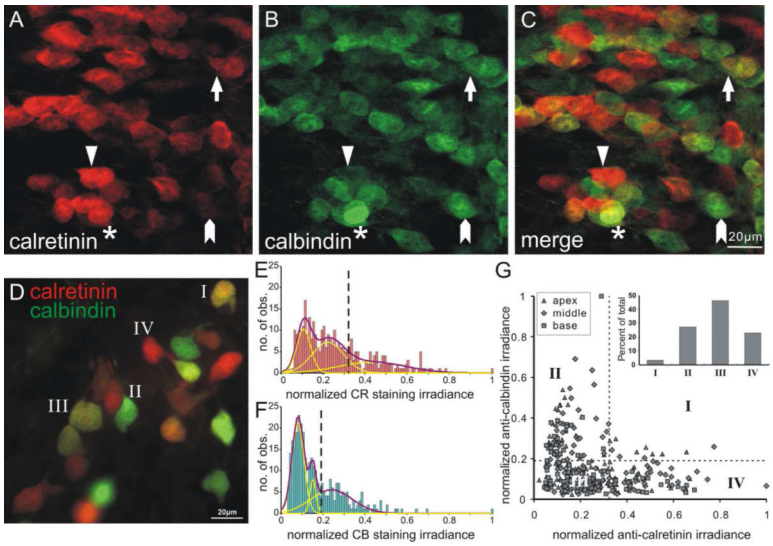

Figure 4. Calretinin and calbindin exhibited differential distribution patterns in murine spiral ganglion

A-C, The mid-cochlear region of a whole-mount preparation of P7 mouse spiral ganglion labeled with mouse anti-calretinin (**A**) and rabbit anti-calbindin (**B**) antibodies. **C,** The merged image of **A** and **B**. Most cells were labeled by mainly calretinin (triangle), mainly calbindin (arrowhead), or a low level of both (arrow). Only a few neurons possessed a high level of both staining (asterisk). Scale bar in **C** (20μm) applies to **A-C**. **D**, Superimposed image of *in vitro* culture shows heterogeneous distribution pattern of calretinin and calbindin that range from mainly calretinin-staining cells (red) to mainly calbindin staining cells (green) similar to **A-C**. Example cells were labeled according to the four categories in **G**. Frequency histograms of normalized calretinin staining irradiance (**E**) and normalized calbindin staining irradiance (**F**) were constructed from measurements of the same single experiment as shown in D (total number of measurements = 320). Both histograms were composed of multiple populations with distinct staining irradiance levels which could be fit by the sum of three Gaussians with discrete means. The vertical dashed lines (**E** and **F**, respectively) delineate the mid points between high and medium means of Gaussian fits of normalized calretinin (0.32) and normalized calbindin (0.19) staining irradiance used in **G** inset. **G**, scatter plot of normalized calretinin and calbindin staining measurements in each neuron. **Inset**, Cells were divided into four categories to highlight relative irradiance patterns based on both x and y cutoffs (dotted lines in **E-F**).

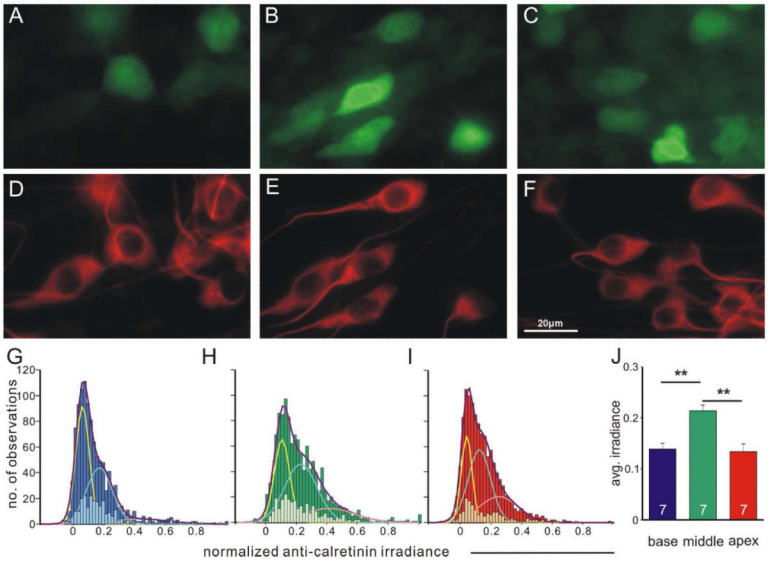

Figure 5. Calretinin staining irradiance is heterogeneous in all tonotopic regions and shows higher average values in the middle region

A-C, Cultured neurons isolated from base, middle and apex respectively, labeled with polyclonal anti-calretinin antibody. **D-F**, same neurons in **A-C** labeled with neuron-specific anti-β-tubulin antibody. Scale bar in **D** applies to **A-F**. **G-I**, Frequency histograms of all data in the seven individual experiments pooled for base (**G**, dark blue bars, total No. of measurements, 1057), middle (**H**, dark green bars, total No. of measurements, 1262) and apex (**I**, dark red bars, total No. of measurements, 1162), fitted by the sum (purple curves) of three Gaussians (yellow, cyan and pink curves) with distinct means, indicating the presence of multiple populations with different calretinin staining levels within each region. Measurements from one representative individual experiment shown as subsets of the pooled data (**G**, light blue bars; **H**, light green bars; **I**, light red bars) displayed similar heterogeneity in all tonotopic positions. **j**, Average calretinin staining irradiance is significantly higher ($p<0.01$) in the middle (n=7).

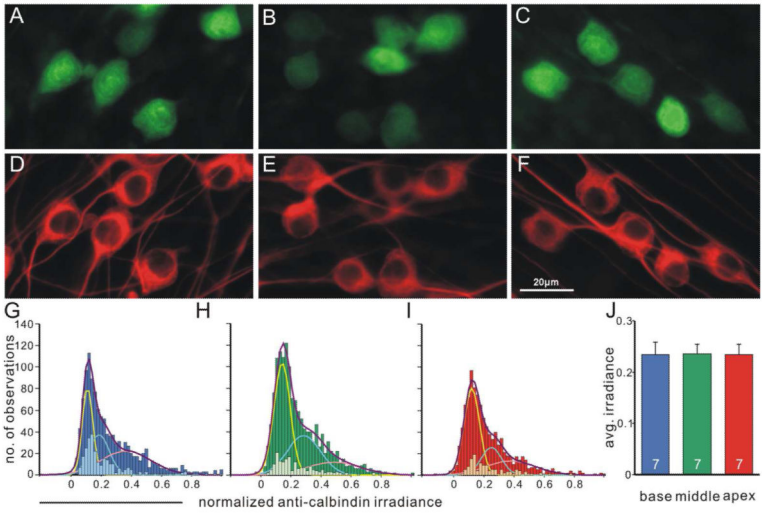

Figure 6. Calbindin staining pattern displays local heterogeneity but is generally even across different tonotopic regions

A-C, Cultured neurons isolated from base, middle and apex respectively, labeled with polyclonal anti-calbindin antibody. **D-F**, Same neurons in **A-C** labeled with neuron-specific anti-β-tubulin antibody. Scale in **F** applies to **A-F**. **G-I**, Frequency histograms of normalized calbindin staining irradiance measurements from seven combined experiments were best fitted by the sum (purple curves) of three Gaussians (yellow, cyan and pink curves) with distinct means for base (**G**, dark blue bars, total No. of measurements, 1156), middle (**H**, dark green bars, total No. of measurements, 1463) and apex (**I**, dark red bars, total No. of measurements, 1018). Data points obtained from a single experiment exhibited as subsets of the full data set in each region and displayed heterogeneity. **J**, average calbindin staining irradiance is comparable in each region (n=7).

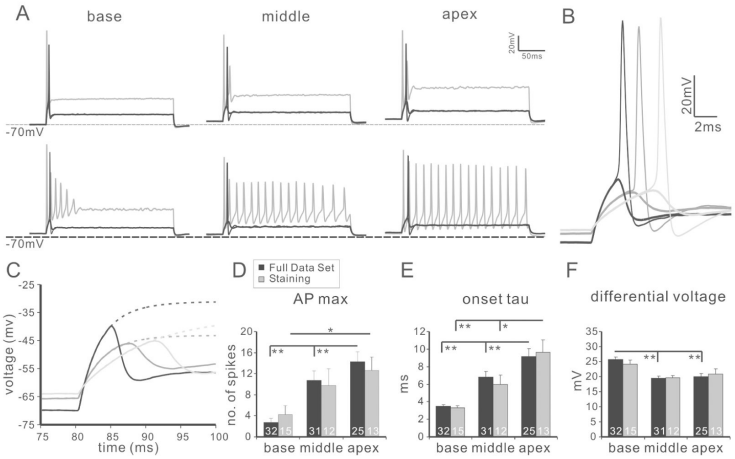

Figure 7. Characterization of spiral ganglion neuron firing properties

A, example traces from base (left panel), middle (middle panel) and apex (right panel) neurons. Both rapidly (upper traces) and slowly (bottom traces) accommodating types of neurons were observed in each region. For each recording, sub-threshold (thick black line), threshold (thin black line) and APmax (gray line) traces are shown as overlay. **B**, overlay of just sub-threshold (thick line) and threshold (thin line) traces from base (black), middle (dark gray) and apex (light gray). **C**, Sub-threshold traces in **B** could be fitted with double exponential functions (dotted line). **D-F**, Tonotopic variation of representative intrinsic firing features. Consistent with previous reports, the accommodation of neuronal firing characterized by AP max (**D**) and the kinetics-related parameter time constant (**E**) was graded linearly from base to apex while excitability-related parameter differential voltage (**F**) showed a non-linear trend across different regions. The full data set (**D-F**, black bars) and a subset of recordings associated with immunostaining measurements (**D-F**, gray bars) showed the same tonotopic trend. *, $p<0.05$; **, $p<0.01$.

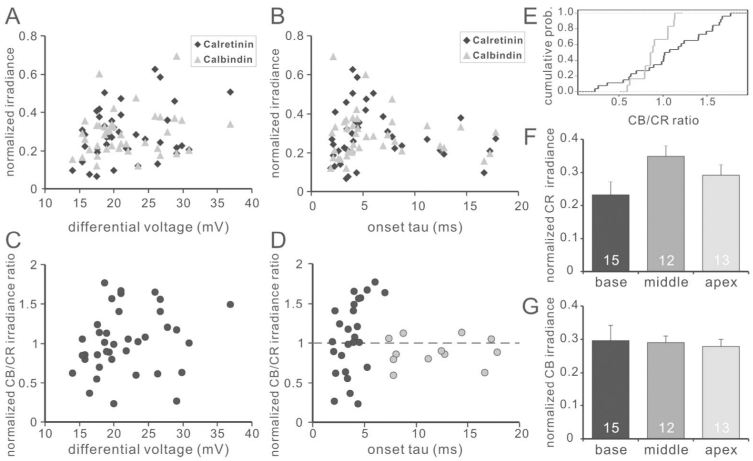

Figure 8. Normalized calbindin/calretinin staining irradiance ratio correlates with action potential kinetics

A-B, relation of calretinin (black diamond) and calbindin (gray triangle) staining irradiance with differential voltage (**A**) and threshold onset time course (**B**). Each data point represents a single recording from one neuron. Neither calretinin nor calbindin staining irradiance correlate with the tested neuronal intrinsic firing properties. **C-D**, Relationship between the ratio of normalized calbindin to calretinin staining irradiance with differential voltage (**C**) and onset tau (**D**). Data from neurons with fast (onset tau< 7.0ms) and slow (onset tau>7.0ms) kinetics were color coded in black and gray, respectively. **E**, Cumulative probability of the normalized calbindin/calretinin staining irradiance of fast (black curve) and slow (gray curve) neurons shown in **D**; two sample Kolomgorov-Smirnov test, $p<0.05$. **F-G**, average calretinin (**F**) and calbindin (**G**) staining irradiance of recorded neurons from different tonotopic regions show a similar trend as in Fig. 4 and Fig. 5.

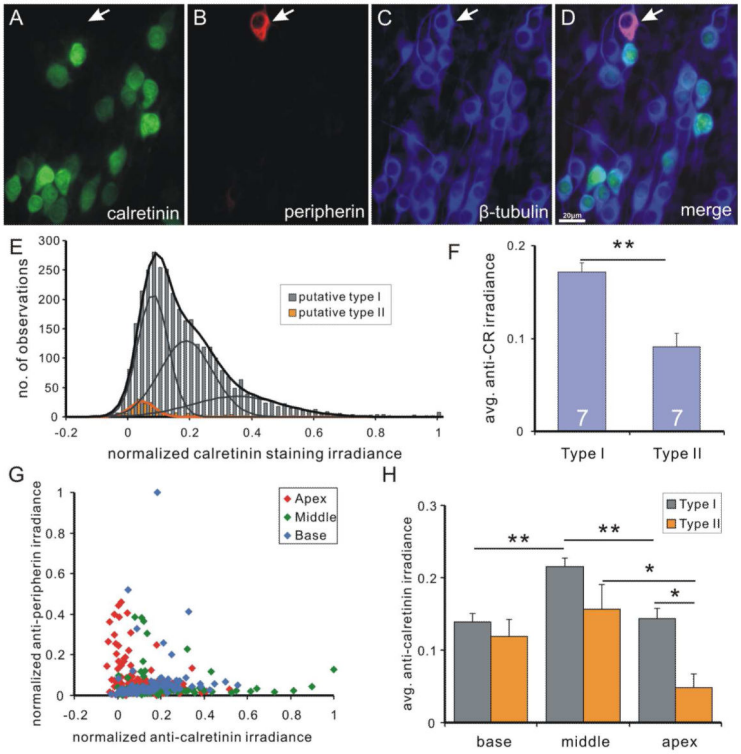

Figure 9. Calretinin staining irradiance is consistently low in putative type II spiral ganglion neurons

A-D, spiral ganglion neurons in a neuronal culture triple-labeled with polyclonal anti-calretinin (**A**), anti-peripherin (**B**) and anti-β-tubulin (**C**) antibodies (**D**, merged image). Calretinin staining irradiance is undetectable in a putative type II neuron (arrow) with high peripherin staining irradiance. **E**, frequency histogram of calretinin staining irradiance measurements from seven pooled experiments. Cells with the highest 5% of peripherin staining irradiance (relative to the total number of neurons) were defined as putative type II neurons. Putative type I neurons (gray bars) are best fitted by the sum (black curve) of three Gaussians (gray curves) and histogram of putative type II neurons (orange bars) is best fitted by a single Gaussian (orange curve). **F**, average calretinin staining irradiance of type I neurons in an entire experiment is significantly higher than that of type II neurons ($p<0.01$, n=7). **G**, scatter plot of normalized calretinin staining irradiance and normalized peripherin staining irradiance from the same experiment as in **E**. **H**, Average calretinin staining irradiance level for type I (gray bars) and type II (orange bars) in different tonotopic regions. *, $p<0.05$, **, $p<0.01$.

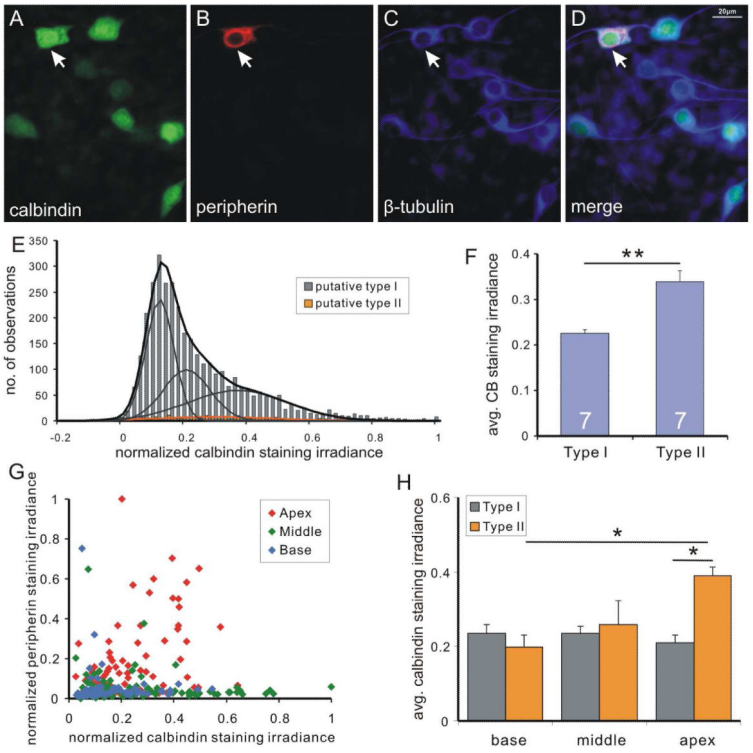

Figure 10. Heterogeneous and generally higher levels of calbindin staining irradiance were observed in type II spiral ganglion neurons

A neuronal culture triple-labeled with polyclonal anti-calbindin (**A**), anti-peripherin (**B**), and anti-β-tubulin (**C**) antibodies (**D**, merged). In contrast to calretinin staining, a putative type II neuron (arrowhead) with high peripherin staining irradiance also had high calbindin staining irradiance. Highest 5% peripherin labeled cells were defined as putative type II neurons. **E**, frequency histogram of calbindin staining irradiance data from seven pooled experiments. Putative type I neurons (gray bars) is best fitted by sum (black curve) of three Gaussians (gray curves) and histogram for putative type II neurons (orange bar) is best fitted by a single Gaussian (orange curve). **F**, average calbindin staining irradiance of type I neurons across all experiments is significantly lower than that of type II neurons ($p<0.01$, n=7). **G**, scatter plot of normalized calbindin and peripherin staining irradiance from an example experiment. **H**, average calbindin staining irradiance level for type I (gray bars) and type II (orange bars) in different tonotopic regions. *, $p<0.05$, **, $p<0.01$.

Table 1

List of Primary Antibodies

Antibody	Immunogen	Manufacturer	Dilution
class III β-tubulin (TUJl)	microtubules derived from rat brain, reactive to neuron specific Class III β-tubulin (βIII)	Covance, MMS-435P	1:200
peripherin	Electrophoretically pure trp-E-peripherin fusion protein, containing all but the 4 N-terminal amino acids of rat peripherin.	Chemicon, MAB1527 Raised in mouse Monoclonal antibody	Basal neurons 1:4000; Middle neurons 1:5000; Apical neurons 1:6000
calretinin	Recombinant rat calretinin	Millipore, AB5054 Raised in rabbit Polyclonal antibody	1:200
calretinin	Recombinant rat calretinin	Millipore, MAB1568 Raised in mouse Monoclonal antibody	1:100
calbindin	Recombinant rat calbindin D-28k (CB)	Swant, CB-38a Raised in rabbit Polyclonal antibody	1:100